

**Best
Available
Copy**

AD-784 723

N_2 SCATTERING MEASUREMENTS AT 10.6
MICRONS

Robert C. Sepucha

Aerodyne Research, Incorporated

Prepared for:

Defense Advanced Research Projects Agency
Office of Naval Research

July 1974

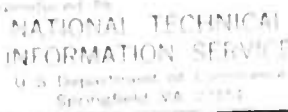
DISTRIBUTED BY:

NTIS

National Technical Information Service
U. S. DEPARTMENT OF COMMERCE
5285 Port Royal Road, Springfield Va. 22151

UNCLASSIFIED

SECURITY CLASSIFICATION OF THIS PAGE (When Data Entered)

REPORT DOCUMENTATION PAGE		READ INSTRUCTIONS BEFORE COMPLETING FORM
1. REPORT NUMBER ARI-RR-51	2. GOVT ACCESSION NO.	3. RECIPIENT'S CATALOG NUMBER AD-784 723
4. TITLE (and Subtitle) N ₂ SCATTERING MEASUREMENTS AT 10.6 MICRONS		5. TYPE OF REPORT & PERIOD COVERED Final Report 11/7/72 - 31/5/74
7. AUTHOR(s) Robert C. Sepucha		6. PERFORMING ORG. REPORT NUMBER
9. PERFORMING ORGANIZATION NAME AND ADDRESS AERODYNE RESEARCH, INC. 20 South Avenue Burlington, Massachusetts 01803		8. CONTRACT OR GRANT NUMBER(s) N00014-73-C-0017 ARPA Order No. 1806 Program Code No. 2E90
11. CONTROLLING OFFICE NAME AND ADDRESS Defense Advanced Research Projects Agency Physical Sciences Division Arlington, Virginia 22217		10. PROGRAM ELEMENT, PROJECT, TASK AREA & WORK UNIT NUMBERS
14. MONITORING AGENCY NAME & ADDRESS (if different from Controlling Office) Office of Naval Research Department of the Navy Arlington, Virginia 22217		12. REPORT DATE July 1974
		13. NUMBER OF PAGES 46
		15. SECURITY CLASS. (of this report) Unclassified
		16. DECLASSIFICATION/DOWNGRADING SCHEDULE
16. DISTRIBUTION STATEMENT (of this Report) This document distributed according to the Distribution List for ARPA Order No. 1806/1807 Unclassified Contracts, dated 1 January 1973		
17. DISTRIBUTION STATEMENT (of the abstract entered in Block 20, if different from Report)		
18. SUPPLEMENTARY NOTES <div style="text-align: center;">  <p>NATIONAL TECHNICAL INFORMATION SERVICE U.S. Department of Commerce Springfield, VA 22151</p> </div>		
19. KEY WORDS (Continue on reverse side if necessary and identify by block number) Rotational Raman Scattering, Rayleigh Scattering, Saturated Absorption, CO ₂ Fluorescence, and CO ₂ ν_3 Rate Constant.		
20. ABSTRACT (Continue on reverse side if necessary and identify by block number) An experimental facility was constructed to measure the molecular scattering cross sections of atmospheric constituents at 10.6 μm . The system was designed to measure the cross sections relative to the radiative lifetime of the 9.4 and 10.4 μm bands of CO ₂ . The calibration procedure included the measurement of CO ₂ fluorescence following laser saturated absorption. (Continued)		

UNCLASSIFIED

SECURITY CLASSIFICATION OF THIS PAGE(When Data Entered)

ABSTRACT (Cont.)

The theory of the experiment and the apparatus are discussed in detail. Data are presented for the N_2 Rayleigh cross section, the smallest quantity measureable with the system. The value of the rate constant for CO_2 (00^0_1) collisional deactivation, measured in the calibration, is also reported.

UNCLASSIFIED

SECURITY CLASSIFICATION OF THIS PAGE(When Data Entered)

N₂ SCATTERING MEASUREMENTS AT 10.6 MICRONS

by Robert C. Sepucha

AERODYNE RESEARCH, INC
Burlington, Massachusetts 01803
Telephone: (617)272-1100

Morton Camac
Principal Investigator

FINAL REPORT

July 1974

Contract No. N00014-73-C-0025

ARPA Order No. 1806
Program Code No. 2E90

Effective Date: 21 July 1972
Expiration Date: 31 May 1974
Amount of Contract: \$119,015

Sponsored by
DEFENSE ADVANCED RESEARCH PROJECTS AGENCY
PHYSICAL SCIENCES DIVISION
Arlington, Virginia 22217

Prepared for
OFFICE OF NAVAL RESEARCH
Department of the Navy
Arlington, Virginia 22217

ABSTRACT

An experimental facility was constructed to measure the molecular scattering cross sections of atmospheric constituents at 10.6 μm . The system was designed to measure the cross sections relative to the radiative lifetime of the 9.4 and 10.4 μm bands of CO_2 .

The calibration procedure consisted of the measurement of CO_2 fluorescence in the 9.4 and 10.4 μm bands following laser saturated absorption. It provided a direct measurement of the sensitivity of the apparatus. In addition, it yielded a rate constant of $k_0 = (1.0 \pm 0.2) \times 10^{-14} \text{ cm}^3/\text{sec}$ for collisional deactivation of CO_2 (00^0_1) in pure CO_2 at 298°K. This is in excellent agreement with the value quoted by Rosser et al. (*J. Chem Phys.*, 50 4996 (1969)).

Based upon this calibration, the N_2 Rayleigh cross section was measured to be $(2.3 \pm 1.4) \times 10^{-33} \text{ cm}^2/\text{sr}$ at 10.6 μm . This is in very good agreement with the value extrapolated to 10.6 μm from measurements made at 6943A by Rudder and Bach (*J. Opt. Soc. Am.*, 58 1260 (1968)). The N_2 rotational Raman scattering level, estimated to be almost two orders of magnitude below the Rayleigh level, was too low to be measured with this facility.

TABLE OF CONTENTS

<u>Section</u>	<u>Page</u>
ABSTRACT	iii
1 INTRODUCTION	1
1.1 Background	1
1.2 Program Objectives and Technical Approach	2
2 THEORY	3
2.1 Introduction	3
2.2 Rayleigh and Raman Scattered Intensities	3
2.3 Optical Filtering of the Rayleigh Component	6
2.4 Dynamic Calibration by Using CO ₂ Fluorescence at 9.4 and 10.4 μm	10
3 EXPERIMENTAL PROGRAM	17
3.1 Description of the Experimental Apparatus	17
3.2 CO ₂ Calibration	23
3.3 N ₂ Rayleigh Scattering	28
3.4 N ₂ Raman Scattering	31
4 CONCLUSIONS	33
5 ACKNOWLEDGMENTS	35
APPENDIX - RADIATIVE LIFETIME IN THE CO ₂ 9.4 AND 10.4 μm BANDS	37
REFERENCES	41

LIST OF ILLUSTRATIONS

<u>Figure</u>		<u>Page</u>
2.1	Rotational Raman Spectrum of Nitrogen at 10.6 μm	8
2.2	CO ₂ Absorption Coefficient at the Center of the P(20) Laser Line at 10.6 μm	9
2.3	Transmission Through Absorption Cell at Center of CO ₂ P(20) Line at 10.6 μm	10
3.1	Schematic of Scattering Cell and CO ₂ Laser	18
3.2	CO ₂ TEA Laser Pulse Shape	20
3.3	Infrared Detection System	22
3.4	Detection Electronics	22
3.5	Typical Oscilloscope Trace for CO ₂ Fluorescence	24
3.6	CO ₂ - ν_3 Deactivation Rate Constant	26
3.7	Comparison of Theoretically Predicted CO ₂ (00 ⁰ 1) Concentration Due to Saturation With Values Deduced From Data	27
A-1	Radiative Lifetime of the 9.4 and 10.4 μm Bands of CO ₂	38

1. INTRODUCTION

1.1 Background

This final report describes the experimental program conducted at Aerodyne Research, Inc., to measure the differential scattering cross sections for N_2 at $10.6 \mu m$. The motivation for the program was to provide fundamental physical data that are required to evaluate the importance of stimulated Raman scattering in degrading high-power CO_2 laser beams as they propagate through the atmosphere.

Probably the most critical limitation on the propagation of pulsed CO_2 beams is due to real air breakdown. This is triggered by atmospheric aerosols present in the path of the laser beam. Such particulate matter can lower the clean air breakdown threshold of 3×10^9 watts/cm² by several orders of magnitude down to approximately 10^7 watts/cm². However, under clean air conditions, when breakdown occurs only for power densities above 10^9 watts/cm², beam degradation may be produced by stimulated Raman scattering.

Raman photons are amplified exponentially by the stimulated scattering process. Consequently, there exists no definitive threshold, as such, for the process. Nonetheless, a useful threshold can be defined as the laser intensity at which the Raman scattered intensity is approximately equal to the incident intensity. This then represents a substantial conversion of laser photons to Raman scattered photons by the stimulated process. Such a threshold is directly proportional to the cross section for spontaneous Raman scattering.

To date, the Raman cross section for the principal atmospheric constituents has been measured only in the visible or near ultraviolet. Measurements at wavelengths longer than $1.0 \mu m$ have not been made. Consequently, values for the cross section at $10.6 \mu m$ must be extrapolated from visible data by the λ^{-4} dependence. This represents an extrapolation over five orders of magnitude, and errors of 20% in the values in the visible become errors of 100% at $10.6 \mu m$. Moreover, the possibility exists of resonance effects enhancing the cross sections of some molecules at $10.6 \mu m$. Therefore, data taken at $10.6 \mu m$ would be preferred.

1.2 Program Objectives and Technical Approach

The goal of the program was to provide the necessary Raman cross section data at $10.6\ \mu\text{m}$. An experimental facility was designed and fabricated to measure the Rayleigh and rotational Raman scattering cross sections for N_2 . The cross section of the entire rotational Raman band was to be measured, and from this, the cross section for each rotational line was to be inferred.

The basic technical approach of the measurement program called for the measurement of the intensity of the Rayleigh- and/or Raman-scattered radiation relative to the intensity of CO_2 fluorescence in its 9.4- and $10.4\text{-}\mu\text{m}$ bands. Consequently, the magnitude of the desired scattering cross sections were to be obtained relative to the well-known CO_2 radiative lifetime. The CO_2 emission was monitored after laser-saturated absorption of the CO_2 gas so that dependence of the CO_2 intensity upon chemical rate constants was avoided. In this way, the infrared detection system was effectively calibrated by the CO_2 emission measurement.

As the measurement program drew to a close, it became apparent from the N_2 Rayleigh scattering data that the rotational Raman scattering intensity was too low to be measurable with this experimental facility. The limit of the range of the facility was reached when the N_2 Rayleigh cross section was measured. For unpolarized laser radiation, that cross section was measured to be $2.3 \times 10^{-33}\ \text{cm}^2/\text{sr}$ at $10.6\ \mu\text{m}$. This is in very good agreement with the values extrapolated from measurements in the visible, using the λ^{-4} dependence of the cross section.

The following section of this report discusses the theory of the measurement. Included are the relationships between measured quantities and the Rayleigh and Raman cross sections. In addition, the calibration procedure employing CO_2 saturated absorption and fluorescence is presented.

In Section 3, the apparatus and the data taken with it are discussed in some detail. The latter include the N_2 Rayleigh cross section and the rate constant for collisional deactivation of $\text{CO}_2(00^0 1)$. Finally, the conclusions are listed in Section 4.

2. THEORY

2.1 Introduction

At 10.6 μm , N_2 has a pure rotational Raman spectrum over which is superimposed the unshifted Rayleigh component. At this wavelength, there is no vibrational Raman component. To determine the cross section for each of these scattering phenomena, the Rayleigh component must be spectrally filtered from the scattered intensity. The following topics are discussed in the present section: the theoretical expressions that relate the total cross section to the parameters measured in the laboratory, the technique by which the Rayleigh component is subtracted from the Raman component, and, finally, the theoretical basis of the calibration by CO_2 fluorescence.

2.2 Rayleigh and Raman Scattered Intensities

For both Rayleigh and Raman scattering, the output voltage produced by the scattered radiation is given by

$$V = R_o I_L \frac{d\sigma}{d\Omega} N \quad , \quad (2-1)$$

where I_L is the incident laser intensity in watts/cm^2 , $d\sigma/d\Omega$ is the differential scattering cross section in cm^2/sr and N is the number density of scatterers in cm^{-3} . The quantity R_o is the overall responsivity of the detection system in $\text{volts}/(\text{watt/cm}^2\text{-sr})$. It takes into account the scattering volume observed by the optical system, the throughput of the optical system, the transmission of any filters that may be in the optical train, the detector responsivity, and the gain of the detector electronics.

For rotational Raman scattering, $d\sigma/d\Omega$ is the cross section for the band, defined by

$$\frac{d\sigma}{d\Omega} N = \sum_J \left(\frac{d\sigma}{d\Omega} \right)_J N_J \quad (2-2)$$

Here, $(d\sigma/d\Omega)_J$ is the differential cross section for the J^{th} rotational line, and N_J is the thermal population of the J^{th} level, where J is the rotational quantum number for the initial level. For diatomic molecules, the differential cross section for the band can be written as^(1,2)

$$\frac{d\sigma}{d\Omega} = \left[(1 - \rho) \cos^2 \psi + \rho \right] \times \sum_J \left\{ \left(\frac{d\sigma}{d\Omega} \right)_J \frac{hcB}{kT} g_J (2J + 1) \cdot \exp \left[- hcBJ (J + 1)/kT \right] \right\} \quad (2-3)$$

where B is the rotational constant, and g_J is the nuclear-statistics factor. For N_2 , $g_J = 6$ when J is even, and $g_J = 3$ when J is odd. The quantity ρ is the depolarization ratio, which for pure rotational Raman scattering is $3/4$.⁽³⁾ The angle ψ is the angle between the electric-field polarization of the incident and scattered radiation.

The cross section per line $(d\sigma/d\Omega)_J$ can be described further as

$$\left(\frac{d\sigma}{d\Omega} \right)_J = K S_{J \rightarrow J \pm 2} (\omega + \Delta\omega_{J \rightarrow J \pm 2})^4 \quad (2-4)$$

Here, K is a constant which includes the anisotropy of the molecular polarizability tensor.⁽⁴⁾ It depends upon the polarization of the incident radiation and the angle at which the scattered radiation is observed. The Placzek-Teller intensity coefficients for a diatomic molecule are⁽⁵⁾

$$S_{J \rightarrow J+2} = \frac{3(J+1)(J+2)}{2(2J+1)(2J+3)} \quad \text{Stokes} \quad (2-5)$$

and

$$S_{J \rightarrow J-2} = \frac{3J(J-1)}{2(2J+1)(2J-1)} \quad \text{Anti-Stokes} \quad , \quad (2-6)$$

where J is the rotational quantum number of the initial state, and $(J \pm 2)$ are the corresponding values for the final state. Finally, the wavelength $\lambda_{J \rightarrow J \pm 2}$ of the scattered radiation is given by

$$\frac{1}{\lambda_{J \rightarrow J \pm 2}} = \frac{1}{\lambda} \pm 4B \left(J + \frac{3}{2} \right) \quad , \quad (2-7)$$

where, again, $(J+2)$ and $(J-2)$ apply to the Stokes and Anti-Stokes lines, respectively. Here λ is the wavelength of the incident radiation.

By combining Eqs. (2-1) through (2-7) at a given temperature, one can determine K from the experimental data for the cross section for the total band, $d\sigma/d\Omega$. Then the differential cross section for each rotational line can be calculated by using Eq. (2-4).

For Rayleigh scattering, the differential cross section is given by⁽⁶⁾

$$\left(\frac{d\sigma}{d\Omega} \right)_{\text{Ray}} = \frac{4\pi^2}{\lambda^4} \left(\frac{n-1}{N} \right)^2 \left(\frac{3}{3-4\rho_v} \right) \left[(1 - \rho_v) \cos^2 \psi + \rho_v \right] \quad , \quad (2-8)$$

for linearly polarized incident radiation. Here, n and N are the refractive index and number density of the scattering medium, respectively, and ρ_v is the depolarization ratio. The angle ψ is the same as defined in Eq. (2-3). For unpolarized incident radiation, the cross section is⁽⁸⁾

$$\left(\frac{d\sigma}{d\Omega} \right)_{\text{Ray}} = \frac{2\pi^2}{\lambda^4} \left(\frac{n-1}{N} \right)^2 \frac{6}{6-7\rho_u} \left[1 + \cos^2 \theta + \rho_u \sin^2 \theta \right] \quad , \quad (2-9)$$

where θ is the angle between the incident and scattered radiation, and ρ_u is the corresponding depolarization ratio. It is related to ρ_v by

$$\rho_u = \frac{2 \rho_v}{1 + \rho_v} \quad (2-10)$$

For $\theta = 90^\circ$ scattering, Eq. (2-9) reduces to

$$\begin{aligned} \left(\frac{d\sigma}{d\Omega} \right)_{\text{Ray}} &= \frac{2\pi^2}{\lambda^4} \left(\frac{n-1}{N} \right)^2 \left(\frac{6 + 6\rho_u}{6 - 7\rho_u} \right) \\ &= \frac{3}{16\pi} \sigma_o \left(\frac{6 + 6\rho_u}{6 - 7\rho_u} \right) \end{aligned} \quad (2-11)$$

where the total cross section per particle, σ_o , is defined as⁽⁹⁾

$$\sigma_o = \frac{32 \pi^3}{3 \lambda^4} \left(\frac{n-1}{N} \right)^2 \quad (2-12)$$

2.3 Optical Filtering of the Rayleigh Component

One of the more troublesome sources of difficulty in the measurement of a rotational Raman cross section is the separation of the Raman component of the scattered intensity from the unshifted Rayleigh component. In the present program, this spectral filtering was to be accomplished in two ways: (1) use of a linearly polarized laser beam, and (2) use of an absorption cell containing hot CO_2 in the path of the scattered radiation.

The advantage of using a linearly polarized laser beam in Raman spectroscopy has been discussed by Weber, et al.⁽¹⁰⁾ The incident laser beam is oriented such that the Raman-scattered radiation is observed normal to the axis of the laser beam in a direction parallel to the polarization vector of the incident radiation. As seen

from Eqs. (2-3) and (2-8), this decreases the Raman and Rayleigh cross sections by ρ and ρ_v , respectively. However, for N_2 , $\rho = 3/4$ and $\rho_v \approx 10^{-2}$, (6, 10, 11) so that the ratio of the Raman to Rayleigh scattered intensities increases by a factor of approximately 10^2 . Extrapolating data obtained with polarized visible radiation to $10.6 \mu m$, one obtains⁽¹²⁻¹⁶⁾ $d\sigma/d\Omega \approx 6.5 \times 10^{-35} \text{ cm}^2/\text{sr}$ for the entire rotational Raman band of N_2 , and^(6, 17) $d\sigma/d\Omega \approx 3 \times 10^{-33} \text{ cm}^2/\text{sr}$ for Rayleigh scattering by N_2 . Therefore, with these depolarization ratios,

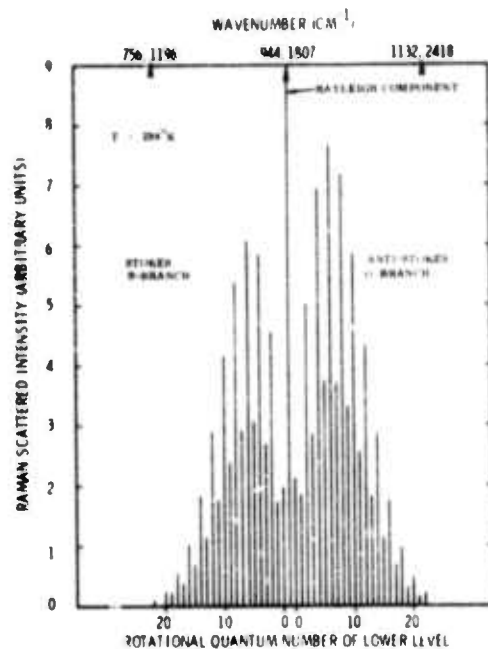
$$\frac{V_{\text{Raman}}}{V_{\text{Rayleigh}}} = \frac{(\rho \, d\sigma/d\Omega)_{\text{Raman}}}{(\rho_v \, d\sigma/d\Omega)_{\text{Rayleigh}}} \approx 1.6 \quad (2-13)$$

The Rayleigh scattered component can be reduced further by inserting a cell of hot CO_2 gas in the path of the scattered radiation in the collection optics. The hot gas acts as a filter to remove both the Rayleigh-scattered radiation and spurious wall scattering. However, since there is virtually no overlap between the rotational Raman spectrum of N_2 and the absorption spectrum of the CO_2 $10.4 \mu m$ band, the Raman-scattered radiation passes through the cell unattenuated.

The rotational Raman spectrum of nitrogen at $10.6 \mu m$ is shown in Fig. 2.1 for $295^\circ K$. The separation of the rotational lines from the Rayleigh fundamental is given by the second term on the right-hand side of Eq. (2-7), i.e.,

$$|\Delta\omega| = 4 B_v \left(J + \frac{3}{2} \right) \quad (2-14)$$

Here, B_v is the rotational constant, and J is the rotational quantum number of the lower level. For N_2 , $B_v = 1.98972 \text{ cm}^{-1}$ for the ground vibrational state,⁽²⁾ so that the spacing between the Rayleigh component and the nearest Raman line ($J = 0$) is 12 cm^{-1} .



AL-510

Figure 2.1 - Rotational Raman Spectrum of Nitrogen at 10.6 μm

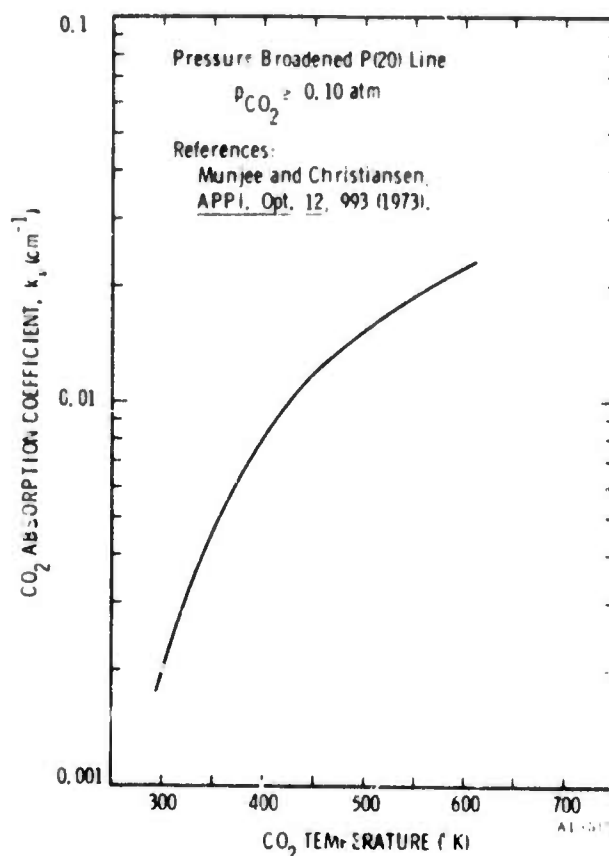
The width of each Raman line is a function of pressure and rotational quantum number, and is given by

$$\Delta\omega = \Delta\omega_0 p \left(\frac{273}{T} \right)^{1/2} \text{ cm}^{-1} \quad (2-15)$$

Here, $\Delta\omega$ is the half-width at half-maximum due to collision broadening, p is the pressure in atmospheres, and T is the temperature in $^{\circ}\text{K}$. The quantity $\Delta\omega_0$ is the broadening coefficient, and has been shown to be a function of quantum number J . For N_2 ,⁽¹⁸⁾ $\Delta\omega_0$ varies from approximately $0.05 \text{ cm}^{-1} \text{ atm}^{-1}$ for $J = 2$ to $0.03 \text{ cm}^{-1} \text{ atm}^{-1}$ for $J = 16$. Therefore, below 10 atm pressure, the overlap of the Raman lines is negligible, and, furthermore, the overlap with the CO_2 absorption lines is small.

Of course, there is exact coincidence between the Rayleigh component and the CO_2 laser line, here taken to be the P(20) line. The absorption coefficient at the center of the P(20) line of CO_2 at 10.6 μm is plotted in Fig. 2.2, as a function of

Figure 2.2 - CO_2 Absorption Coefficient at the Center of the P(20) Laser Line at $10.6 \mu\text{m}$



gas temperature.⁽¹⁹⁾ The corresponding transmission for a 370 cm path is plotted in Fig. 2.3, as a function of CO_2 gas temperature. Above about $5 \times 10^{-2} \text{ atm}$ of CO_2 , the line becomes purely collision-broadened, so that these results are independent of gas pressure above 10^{-1} atm . Indicated in Fig. 2.3 is the operating level for the CO_2 absorption cell to suppress the N_2 Rayleigh scattering below 10% of the total Raman scattering, after Eq. (2-13) is taken into account. A gas temperature of approximately 350°K is required. For the Rayleigh component to be only 1% of the Raman intensity, a gas temperature of 440°K is necessary.

Therefore, with a linearly polarized laser and a hot CO_2 filter, it is possible to eliminate the Rayleigh component of radiation scattered by N_2 at $10.6 \mu\text{m}$. The degree to which the Raman component is also absorbed by the CO_2 filter can be determined by measuring the scattered intensity as a function of CO_2 temperature.

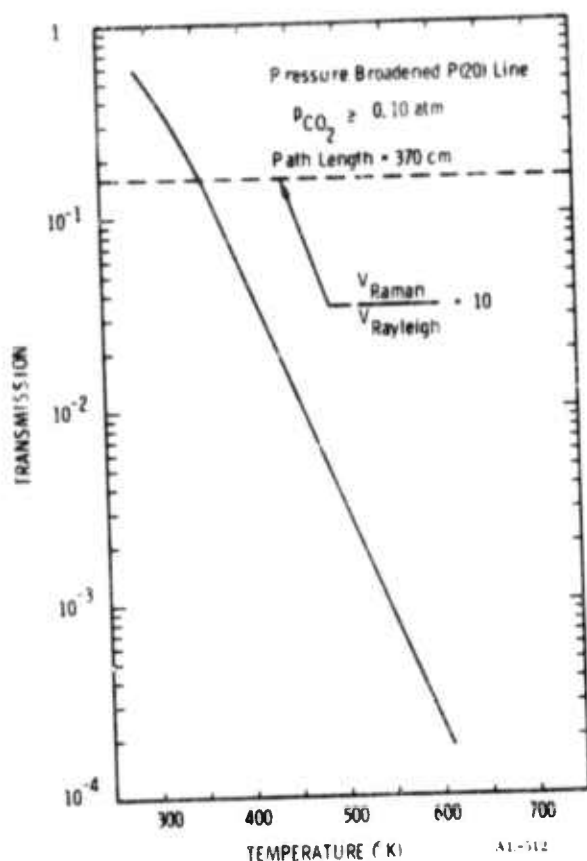


Figure 2.3 - Transmission Through Absorption Cell at Center of CO_2 P(20) Line at $10.6 \mu\text{m}$. The scattering signals apply for a linearly polarized laser beam.

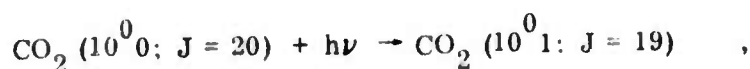
2.4 Dynamic Calibration by Using CO_2 Fluorescence at 9.4 and $10.4 \mu\text{m}$

The cross section of the rotational Raman band can be measured relative to the Rayleigh cross section if data are acquired both with and without linearly polarized radiation and with and without the CO_2 filter. The absolute Raman cross section can then be obtained by calculating the Rayleigh cross section from Eq. (2-11). To eliminate the assumptions implicit in these calculations, however, the experimental system must be calibrated. This calibration then allows the Rayleigh and Raman cross sections to be measured directly.

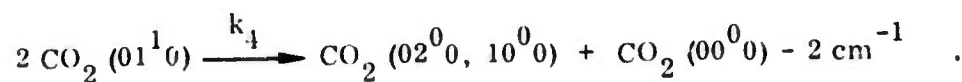
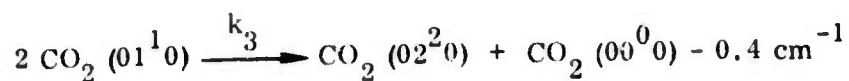
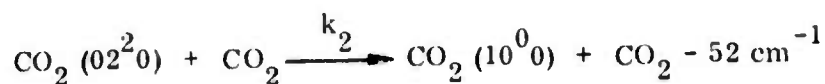
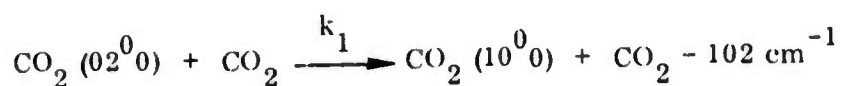
The method chosen to calibrate the system is the measurement of the intensity of the well-known CO_2 fluorescence in the 9.4 and $10.4 \mu\text{m}$ bands, which follows the saturated absorption of laser radiation by the gas. This technique uses the same optical system as the Raman and Rayleigh measurements, and is performed over approximately the same time scale. It eliminates the need to calculate the scattering volume observed by the optical system, the optical throughput, and the detector responsivity; i.e., the calibration directly determines the system responsivity, R_o .

A critical feature of the dynamic calibration is the fact that the incident-laser power density is sufficiently high in the apparatus ($I_L \approx 10^7$ to 10^8 watts/cm²) to saturate the absorbing CO₂ (10⁰0; J = 20) level. Consequently, the population of the entire CO₂ (00⁰1) vibrational state at the end of the laser pulse is independent of the absolute magnitude of the rate constants for the kinetic processes involving the states of interest. Only the relative magnitudes of these rate constants are important.

During the laser pulse, the population of the CO₂ (00⁰1) state increases by



while the population of the absorbing CO₂ (10⁰0) state is replenished by



The rate constants for these processes at 298⁰K are^(20, 21)

$$k_1 = 1.8 \times 10^{-11} \text{ cm}^3/\text{sec} ,$$

$$k_2 = 2.3 \times 10^{-11} \text{ cm}^3/\text{sec} .$$

$$k_3 = 1.0 \times 10^{-11} \text{ cm}^3/\text{sec} ,$$

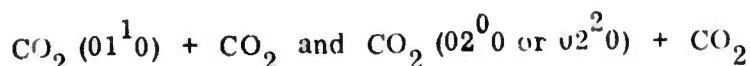
$$k_4 = 7.5 \times 10^{-13} \text{ cm}^3/\text{sec} ,$$

so that the characteristic times for the reactions are

$$\begin{aligned} \tau_1 &= \frac{2.3 \times 10^{-9}}{p_{\text{CO}_2}} & , & & \tau_3 &= \frac{5.5 \times 10^{-9}}{p_{\text{CO}_2}} & , \\ \tau_2 &= \frac{1.8 \times 10^{-9}}{p_{\text{CO}_2}} & , & & \tau_4 &= \frac{7.4 \times 10^{-7}}{p_{\text{CO}_2}} & , \end{aligned}$$

where p_{CO_2} is the pressure in atmospheres. The fourth reaction then can be neglected for present purposes when $p_{\text{CO}_2} < 0.4$ atm. Nevertheless, the $\text{CO}_2(01^10)$ state is strongly coupled to the absorbing state because of the third reaction.

The repopulation of the $\text{CO}_2(02^00)$ and $\text{CO}_2(02^20)$ states by



has a characteristic time of 90 μsec at $p_{\text{CO}_2} = 1$ atm, and, consequently, is not important during the ~ 2 μsec laser pulse. The repopulation of the $\text{CO}_2(01^10)$ state from the ground state is even slower (180 μsec at $p_{\text{CO}_2} = 1$ atm), so that the $\text{CO}_2(10^00)$ state is effectively decoupled from the ground state. Therefore, for CO_2 pressures between approximately 10^{-3} and 20 atm, the populations of the $\text{CO}_2(10^00)$, $\text{CO}_2(02^00)$, $\text{CO}_2(02^20)$, and $\text{CO}_2(01^10)$ states are closely coupled, while at the same time being decoupled from the ground state. The effective population of the lower level for laser-saturated absorption, then, is the sum of the populations of these four states.

For saturated absorption in a molecular system such as CO_2 , kinetic rate equations must be written for all the molecular levels coupled to the lower absorbing level. The rate of depletion of the lower level due to absorption and, consequently, the rate of population of the upper level, are governed by the term⁽¹⁰⁾

$$\sigma \delta \int_0^{t_L} \frac{I_L}{h\nu} dt = \sigma \delta \frac{E_L}{h\nu A_L} .$$

Here, σ is the absorption cross section for the transition and t_L , E_L , and A_L are the pulse width in seconds, the energy in joules, and the beam cross sectional area in square centimeters respectively, for the laser pulse. The quantity δ is the ratio of the population of the $\text{CO}_2(10^0_0; J=20)$ level to that for all the other levels strongly coupled to it; i.e., for the present case,

$$\delta \equiv \left[\text{CO}_2(10^0_0; J=20) \right] \left\{ \left[\text{CO}_2(10^0_0) \right] + \left[\text{CO}_2(02^0_0) \right] + \left[\text{CO}_2(02^2_0) \right] + \left[\text{CO}_2(01^1_0) \right] \right\}^{-1} \quad (2-16)$$

The more complex that the molecular systems is, i.e., the more levels coupled to the absorbing level, the more difficult it is to attain full saturation. In this sense, saturation is achieved when

$$2\sigma\delta \frac{E_L}{h\nu A_L} > 1 \quad (2-17)$$

When this condition is satisfied, the population of the upper level at the end of the laser pulse, $[\text{CO}_2(00^0_1)]_L$, is given by

$$\begin{aligned} [\text{CO}_2(00^0_1)]_L &= [\text{CO}_2(10^0_0)] = [\text{CO}_2(02^0_0)] \exp\left[-\frac{(E_{10^0_0} - E_{02^0_0})}{kT}\right] \\ &= [\text{CO}_2(02^2_0)] \exp\left[-\frac{(E_{10^0_0} - E_{02^2_0})}{kT}\right] \\ &= [\text{CO}_2(01^1_0)] \exp\left[-\frac{(E_{10^0_0} - E_{01^1_0})}{kT}\right] \end{aligned} \quad (2-18)$$

where $E_{01^1_0}$, $E_{02^2_0}$, $E_{02^0_0}$, and $E_{10^0_0}$ are the vibrational energies of the respective states. Coupled with the fact that

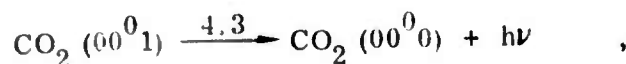
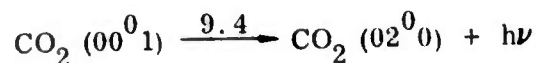
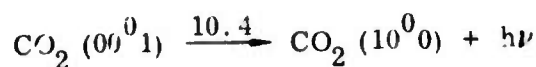
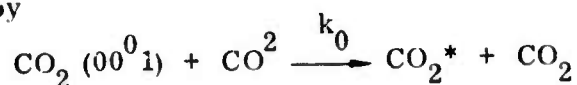
$$\begin{aligned}
& [\text{CO}_2 (00^0 1)] + [\text{CO}_2 (10^0 0)] + [\text{CO}_2 (02^2 0)] + [\text{CO}_2 (02^0 0)] + [\text{CO}_2 (01^1 0)] \\
& = \left\{ [\text{CO}_2 (00^0 1)] + [\text{CO}_2 (10^0 0)] + [\text{CO}_2 (02^2 0)] + [\text{CO}_2 (02^0 0)] \right. \\
& \quad \left. + [\text{CO}_2 (01^1 0)] \right\}_{\text{equil}} \quad . \quad (2-19)
\end{aligned}$$

the $\text{CO}_2 (00^0 1)$ population at the end of the laser pulse can be expressed as

$$[\text{CO}_2 (00^0 1)]_L = 5.20 \times 10^{16} p_{\text{CO}_2} \quad (2-20)$$

at 298°K.

The magnitude of $[\text{CO}_2 (00^0 1)]_L$ determines the intensity of the subsequent fluorescence. Immediately following the laser pulse, the $\text{CO}_2 (00^0 1)$ population is decreased by



where CO_2^* represents $\text{CO}_2 (01^1 0, 02^0 0, 10^0 0, 11^1 0, \text{ or } 03^1 0)$. The radiative lifetimes for the three emission bands are⁽²²⁾ $\tau_{10.4} \approx \tau_{9.4} = 5.0$ sec, and⁽²³⁾ $\tau_{4.3} = 2.4 \times 10^{-3}$ sec, respectively, and the rate constant for collisional deactivation is⁽²⁴⁻²⁷⁾ $k_0 = 1 \times 10^{-14}$ cm³/sec at 298°K. Therefore, after the laser pulse, the CO_2 excited-state population is

$$[CO_2 (00^0 1)] = [CO_2 (00^0 1)]_L e^{-t/\tau} , \quad (2-21)$$

where

$$\begin{aligned} \frac{1}{\tau} &= k_0 [CO_2] + \frac{1}{\tau_{4.3}} + \frac{1}{\tau_{9.4}} + \frac{1}{\tau_{10.4}} \\ &\approx k_0 [CO_2] = 2.5 \times 10^5 p_{CO_2} . \end{aligned} \quad (2-22)$$

The dynamic calibration consists of measuring the CO_2 emission following the laser pulse. The voltage output of the detection system is given by

$$V_{CO_2} = R_o [CO_2 (00^0 1)]_L e^{-t/\tau} S_{CO_2} , \quad (2-23)$$

where S_{CO_2} is the emission from CO_2 in watts/sr. For the 9.4 and 10.4 μm bands, S_{CO_2} is given by the equation

$$S_{CO_2} = \frac{hc}{4\pi} \sum_{J'} \frac{1}{\lambda_{J'} \tau_{J'}} \frac{[CO_2 (00^0 1; J')]}{[CO_2 (00^0 1)]} , \quad (2-24)$$

where h is the Boltzmann constant, J' is the rotational quantum number of the upper state, and $\lambda_{J'}$ and $\tau_{J'}$ are the corresponding wavelength and radiative lifetimes, respectively, for the particular rotational line. The summation extends over the P and R branches of both bands, and includes the fact that only odd J 's are symmetry allowed.

The radiative lifetimes, $\tau_{J'}$, can be determined from measured band intensities, as is shown in the Appendix. Alternatively, since the intensities of the two bands are similar, a mean lifetime per line, $\tau_r \approx 5$ sec, and a mean wavelength, $\bar{\lambda} \approx 10 \mu m$, can be used in Eq. (2-24) with very little loss in accuracy (see the Appendix). In this case, the expression for S_{CO_2} reduces to

$$S_{\text{CO}_2} \approx \frac{4hc}{4\pi \bar{\lambda} \tau_r} = 1.27 \times 10^{-21} \text{ watt/sr} ,$$

the factor of 4 in the numerator accounting for the fact that there are two bands, each of which consists of a P and R branch.

The CO_2 fluorescence signal becomes

$$\begin{aligned} V_{\text{CO}_2} &= R_o \frac{4hc}{4\pi \bar{\lambda} \tau_r} \left[\text{CO}_2 (00^0_1) \right]_L e^{-t/\tau} \\ &= 1.27 \times 10^{-21} R_o \left[\text{CO}_2 (00^0_1) \right]_L . \end{aligned} \quad (2-25)$$

The CO_2 calibration, then, consists of two simultaneous measurements which provide information on both the time response and the absolute sensitivity of the detection system. The temporal decay of V_{CO_2} yields the relaxation time τ , and a rate constant k_0 which can be compared with the published values.⁽²⁴⁻²⁷⁾ More importantly, the calibration yields the system responsivity R_o , which is necessary to determine the scattering cross section, $d\sigma/d\Omega$, from Eq. (2-1).

3. EXPERIMENTAL PROGRAM

The measurement program consisted of a dynamic calibration using CO_2 9.4 and 10.4 μm fluorescence, and the observation of scattered radiation from N_2 . The apparatus required to perform these measurements was described in detail in the previous report.⁽²⁸⁾ However, since that time, several changes have been made, and data have been taken. In this section is presented a description of the modified apparatus used in the program, with reference to the previous description⁽²⁸⁾ whenever possible. The data obtained with the system are then discussed.

3.1 Description of the Experimental Apparatus

The system consisted of four major components: a CO_2 laser, a scattering cell, an absorption cell in the optical train, and an infrared detector with associated electronics. A schematic diagram of the scattering cell is shown in Fig. 3.1. The cell was a 12-in. diameter, 96-in. long, steel chamber capable of withstanding internal pressures of 4 atm. It contained optical mounts which held a 2-in. diameter, 1m focal-length KCl lens and a 2-in. diameter, 1m radius-of-curvature, gold coated total reflector. The reflector formed one end of the CO_2 laser cavity, and with the lens, focused the laser beam to a minimum cross section at the center of the cell. The entrance window of the cell was a 2.5-in. diameter KCl flat, and the observation port, located opposite the focal volume, was a 4.25-in. diameter KCl flat.

To suppress wall scattering, 12 Mylar baffles were inserted in the cell along the laser axis and along the detector line-of-sight. The apertures for the baffles ranged from 5 to 10 cm in diameter. With such an arrangement, we were capable of suppressing the wall scattering to approximately 10^{-11} to 10^{-12} of the incident beam intensity.

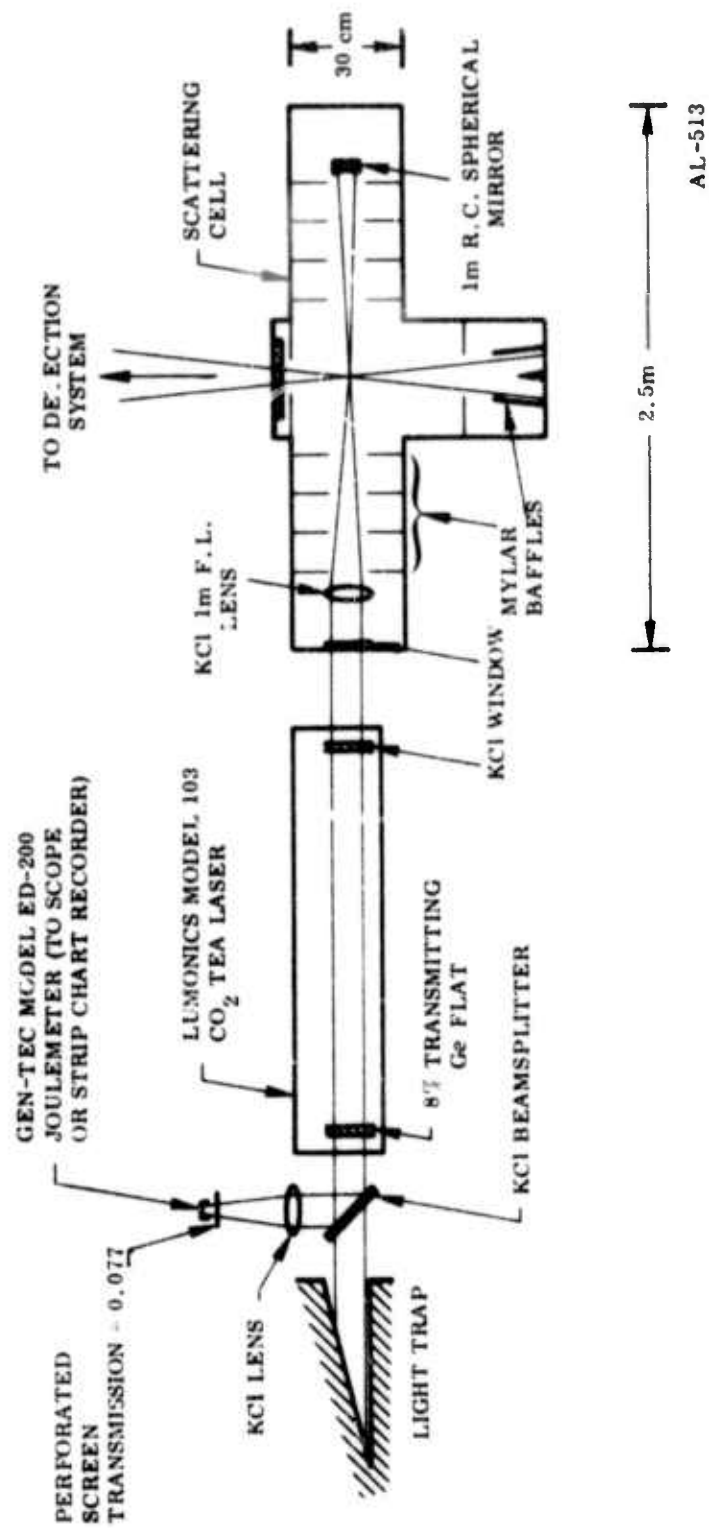


Figure 3.1 - Schematic of Scattering Cell and CO₂ Laser

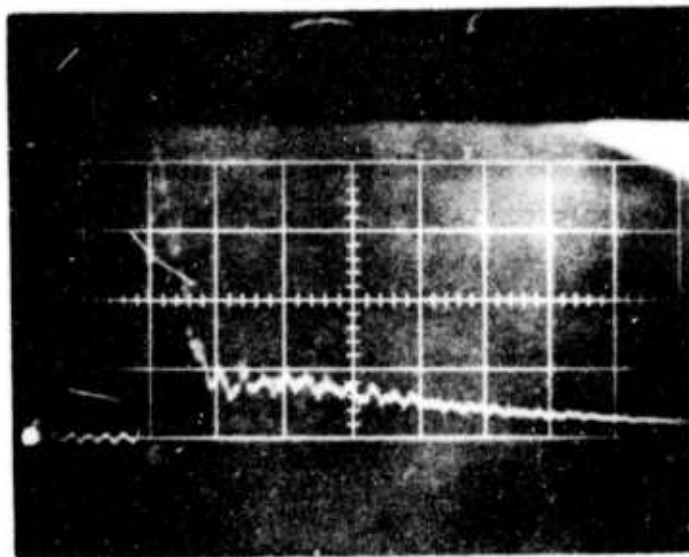
The cell could be evacuated to 3 torr with a mechanical pump, with the pressure being read on a Wallace-Tiernan Model FA 160 high precision vacuum gauge. Pressures above 1 atm were recorded on a Matheson Model 63-5642 high pressure gauge. The gases entering the cell were passed through a Millipore filter containing an 0.80 μm pore prefilter and a 0.025 μm pore filter element. This filtering was found sufficient to remove almost all the dust in the gases entering the cell. The primary problem that arose was dust already in the cell producing laser breakdown. This occurred after several laser shots (~ 300), regardless of the number of times the cell was flushed. This supports the speculation that dust on the optical elements was being blown off after several shots, and was causing the breakdown.⁽²⁹⁾

The CO_2 laser was a Lumonics Model 103 TEA laser, which operated on the P(20) line at 10.6 μm . The output mirror of the laser was a coated germanium flat with a reflectivity of approximately 90%. The output energy was monitored with a Gen-Tec Model ED-200 joulemeter. The factory calibrated instrument had a sensitivity of 10.9 volt/joules when used with a $10^6 \Omega$ load. To avoid damaging the sensitive element of the joulemeter, the focused laser beam was attenuated by metal screens manufactured by Perforated Products, Inc. The screens had calibrated transmissions ranging from 2% to 30%. The signal from the joulemeter was both observed on an oscilloscope and recorded on a strip chart recorder.

The temporal shape of the laser pulse was observed with an Oriel Corporation, Model 7411, photon drag detector. The typical TEA-laser pulse shape is shown in Fig. 3-2. It consists of an initial spike 0.20 μsec wide, followed by a long tail lasting an additional 2.3 μsec . Approximately 40% of the pulse energy was contained in the initial spike.

The laser pulse repetition rate was one pulse per second, and the unpolarized output was nominally 1.5 joules per pulse in the configuration described above. The output had a measured reproducibility of 5 to 10% over a span of 75 to 100 consecutive pulses.

Reproduced from
best available copy.



AL-514

Figure 3.2 - CO₂ TEA Laser Pulse Shape

The laser output was monitored with the joulemeter for every shot for which CO₂ or N₂ data were taken. The energy measured by the joulemeter, E_{out} , can be related to the one-way energy flux, E_1 , inside the laser cavity by $E_{out} = 0.088E_1$, since the transmission of the laser output mirror was 8.8%. Similarly, the two-way energy flux, E_L , in the cavity is related to E_1 by $E_L = 1.908E_1$, since the reflectivity of the output mirror was 90.8%. Consequently, the two-way flux is

$$E_L = 21.68 E_{out} \quad (3-1)$$

The perforated screen and the KCl beamsplitter in front of the joulemeter had a measured transmission of 7.7% and reflectivity of 10.5%, respectively. Thus, since the joulemeter sensitivity was 10.9 volt/joules, the output of the joulemeter, V_L in volts, was related to the laser cavity flux by

$$E_L = V_L (0.077) (0.105) (10.9) \quad ; \quad (3-2)$$

$$E_L = 246 V_L \quad \text{joules} \quad ,$$

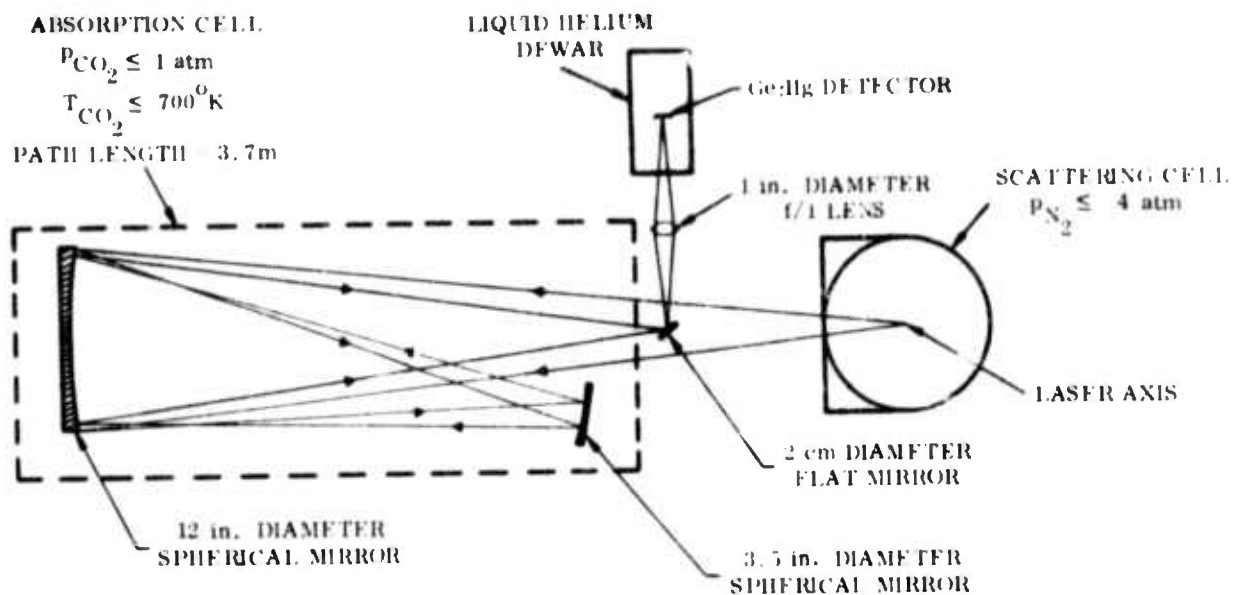
since under these conditions, $E_{out} = 11.35 V_{out}$. Therefore, for a joulemeter output of 132 mv, the output energy is 1.5 joules and the intracavity flux is 32.5 joules.

The laser spot size in the focal plane was measured by inserting apertures in the path of the beam. The size of the apertures was increased until the laser output was the same as that measured with no apertures present. In this manner, the laser beam was found to have a rectangular cross section 0.83×0.36 cm, with the major axis lying in the horizontal scattering plane. Thus, the beam area at the focal plane was $A_L = 0.3 \text{ cm}^2$. For a laser pulse for which $E_L = 32.5$ joules, this corresponds to a peak power density of $I_L \approx 4 \times 10^8 \text{ watts/cm}^2$ in the cavity.

A schematic drawing of the detection system is shown in Fig. 3.3. The radiation scattered 90° from the laser axis was collected by a 12-in. diameter, gold coated spherical mirror located approximately 1.5m from the laser axis. This represented a solid angle of 3.1×10^{-2} sr. The mirror was contained in the 3.7m, folded-path absorption cell described previously.⁽²⁸⁾ The radiation emerging from the absorption cell was focused onto an infrared detector with a one-inch diameter, f/1 lens made of Irtran II. The detector, also described previously,⁽²⁸⁾ was a mercury-doped-germanium, infrared detector, purchased from the Santa Barbara Research Center. Its peak responsivity at $11 \mu\text{m}$ was 24.36 amp/watt.

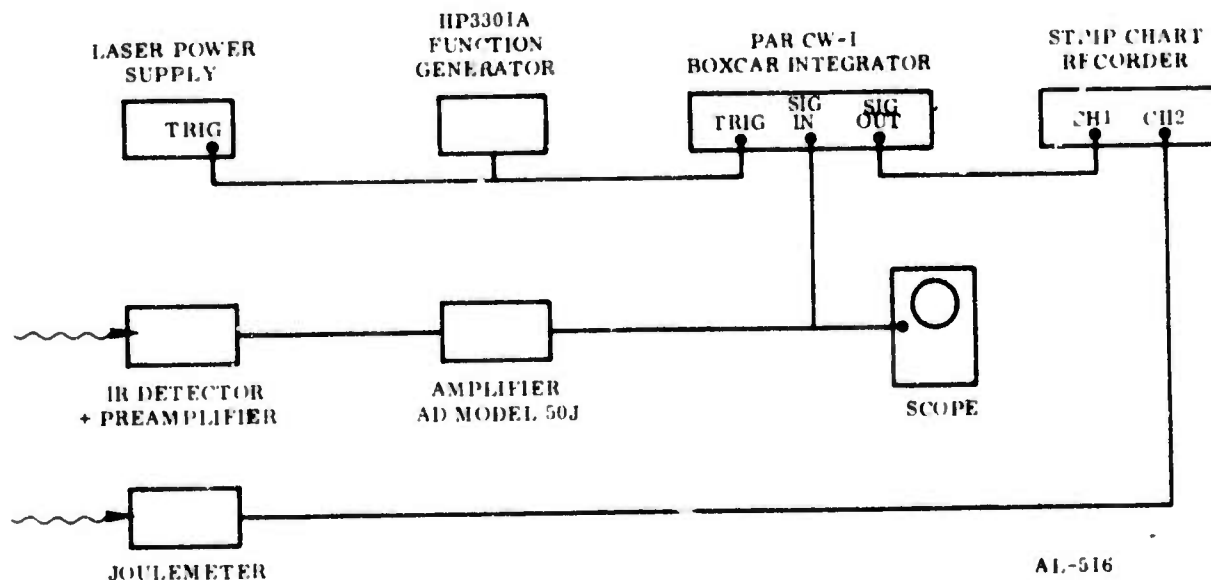
The output of the detector was fed directly into a preamplifier constructed at Aerodyne Research, Inc.⁽²⁸⁾ The unit had a voltage gain of 42 and a bandwidth of 6.7 corresponding to an RC time constant of 24 nsec.

For CO_2 calibration runs in which the decay of the CO_2 fluorescence was measured, the output of the preamplifier was monitored on a Type 585 Tektronix oscilloscope. However, for the CO_2 calibration runs in which the system responsivity was measured and for the N_2 scattering runs, the signal from the preamplifier was processed with the instrumentation shown schematically in Fig. 3.4. The output of



AL-515

Figure 3.3 - Infrared Detection System



AL-516

Figure 3.4 - Detection Electronics

the preamplifier was fed into a Model 50J, Analog Devices, Inc., amplifier, which had a gain of 10 and a bandwidth of 8 MHz. The output of this amplifier was then fed into a Model CW-1 boxcar integrator, manufactured by Princeton Applied Research, Inc. The outputs from both the boxcar integrator and the joulemeter were recorded on a dual-channel Leeds and Northrup Model XL-602 strip chart recorder.

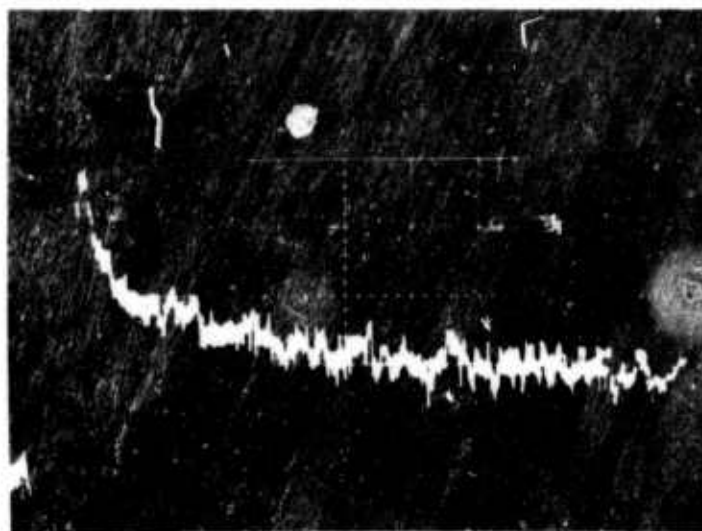
The procedure for taking data started with preliminary measurements of the responsivity, R_0 , by using CO_2 fluorescence. When the optical system was aligned (determined when R_0 was maximized), the time decay of the fluorescence was measured. This gave τ and k_0 . The measurement of R_0 was then repeated. On any given day when N_2 scattering data were taken, R_0 was measured both immediately before and after the N_2 runs.

3.2 CO_2 Calibration

The basic procedure used to check the alignment of the apparatus was the calibration by CO_2 fluorescence. For this case, the scattering cell was evacuated to approximately 3 torr before being filled to the desired pressure with CO_2 . When operating at pressures near 1 atm, care had to be taken to flush the scattering cell two or three times before taking data in order to avoid laser breakdown. Despite this precaution, however, breakdown occurred after 10 to 20 laser shots when the pressure was 1 to 2 atm. When this happened, the cell had to be flushed and refilled before the measurement could be resumed. All measurements were made at room temperature, $298 \pm 2^\circ\text{K}$.

For the calibration, the laser radiation was unpolarized, and the laser energy in the cavity ranged from 30 to 40 joules per pulse. This corresponds to peak power densities at the focal volume of about 5×10^8 watts/cm². The absorption cell in the optical path between the scattering cell and the infrared detector was left open to room air, and consequently had no effect on the measured intensities.

As mentioned in the previous subsection, the output of the detector preamplifier was monitored directly on a Type 585 Tektronix oscilloscope. A typical trace for such a run is shown in Fig. 3.5. The first 5 μsec of the signal was due to wall



CO₂ PRESSURE: 0.25 atm AL-517
 VERTICAL: 200 mV/cm
 HORIZONTAL: 5 μsec/cm

Figure 3.5 - Typical Oscilloscope Trace for CO₂ Fluorescence

scattering of the laser radiation in the scattering cell. However, the remainder of the pulse decayed exponentially with time and was due to CO₂ fluorescence. The random noise component of the signal was approximately 0.12v, and was due to intrinsic generation-recombination noise in the infrared detector.

The observed fluorescent intensity was attributed to the 9.4 and 10.4 μm bands of CO₂. There was no contribution from the 4.3 μm band, since emission in that band was reabsorbed by the CO₂ in that part of the scattering cell lying in the field-of-view of the detector, between the laser axis and the observation port. The distance through undisturbed CO₂ along that path was 30 cm. Therefore, the mean transmission at 0.10 atm of CO₂ was 10⁻⁶⁶ at 4.3 μm, since the absorption coefficient is approximately 50 cm⁻¹-atm⁻¹ at room temperature.⁽³⁰⁾ For the 9.4 and 10.4 μm bands, however, the transmission was 94% over the same path.

For each calibration run, the signal strength was read directly from oscilloscope photographs. The results were a least-squares fit to the expression $V_{\text{CO}_2} = C \exp(-t/\tau)$, where C is a constant at each pressure. The CO_2 ν_3 deactivation rate constant was then calculated from

$$k_0 = \frac{1}{[\text{CO}_2]\tau} = \frac{4.06 \times 10^{-20}}{p_{\text{CO}_2} \tau}, \quad (3-3)$$

where p_{CO_2} is the gas pressure in atm, and τ is in seconds. The results determined in this manner for over fifty individual runs are shown in Fig. 3.6 for pressures from 0.25 to 2.0 atm. For this range, the relaxation time, τ , assumed values from approximately 16 to 2 μsec . Several data points at the same pressure indicate data taken on different days. The error bars represent the standard deviation for the particular set of runs. The mean value of all the data points, $k_0 = (1.0 \pm 0.2) \times 10^{-14} \text{ cm}^3/\text{sec}$, is in agreement with the previously published values at 298°K. A comparison with these values is shown in Table 3.1.

The absolute intensity of the CO_2 fluorescence was measured by using both oscilloscope traces and the boxcar integrator. The system sensitivity was then determined from Eq. (2-25) with Eq. (2-20). The condition in Eq. (2-17) must be satisfied to allow Eq. (2-20) to be used for $[\text{CO}_2 (00^0 1)]_L$. For the pressure broadened P(20) line, the absorption cross section is given by

$$\sigma = \frac{k_\nu}{[\text{CO}_2 (10^0 0)]} = \frac{6.65 \times 10^{-20}}{p_{\text{CO}_2}} \text{ cm}^2,$$

since the absorption coefficient at the line center is⁽³¹⁾ $k_\nu = 1.84 \times 10^{-3} \text{ cm}^{-1}$ at 298°K. Therefore, for $E_L = 40\text{J}$, $A_L = 0.3 \text{ cm}^2$, and the 298°K equilibrium value $\delta = 8.9 \times 10^{-4}$, the condition in Eq. (2-17) becomes

$$p_{\text{CO}_2} < 0.7 \text{ atm.}$$

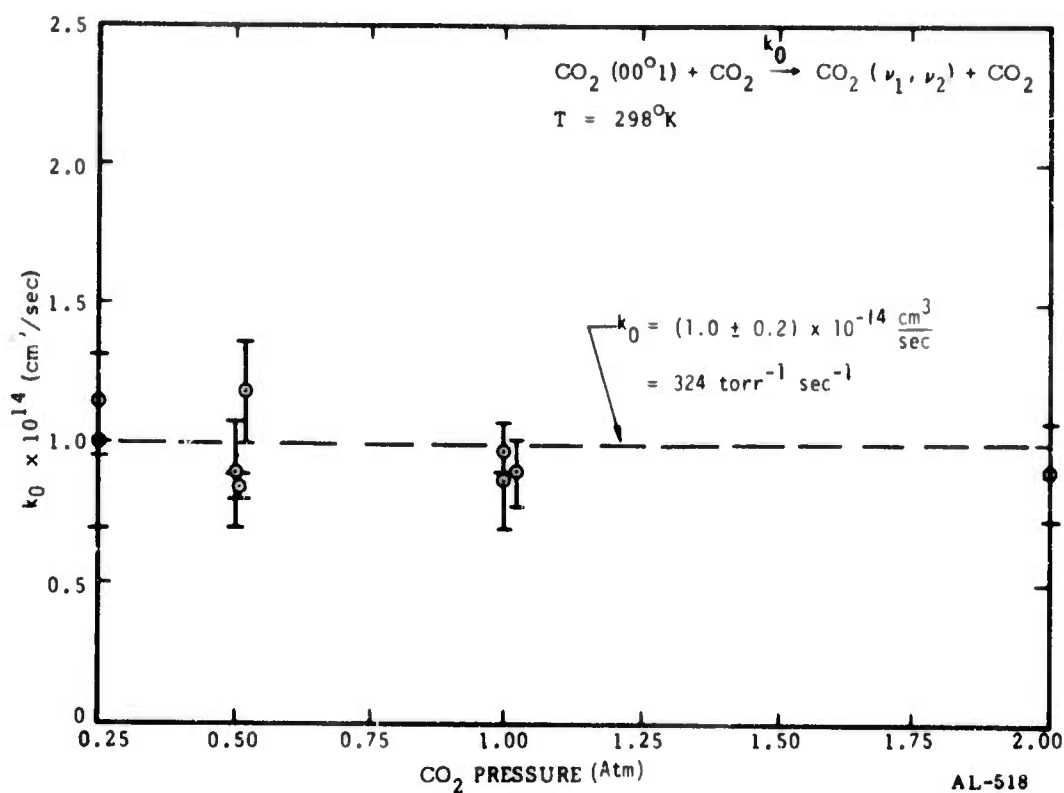
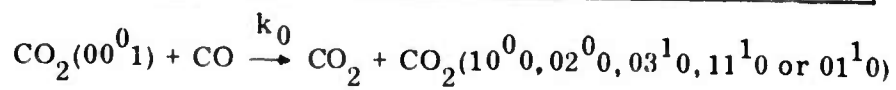


Figure 3.6 - $\text{CO}_2 - \nu_3$ Deactivation Rate Constant

TABLE 3.1

$\text{CO}_2(\nu_3 = 1)$ DEACTIVATION RATE CONSTANT AT 300°K

$k_0(\text{cm}^3 - \text{sec}^{-1})$	Reference
1.02×10^{-14}	24, 25
1.09×10^{-14}	26, 27
1.0×10^{-14}	Present Study



The results of a typical set of runs with pressures in the range of 0.067 to 0.52 atm and $E_L = 44\text{J}$, gave $R_0 = 1.96 \times 10^4 \text{ volts/watts-cm}^{-3}\text{-sr}^{-1}$, with a standard deviation of $\pm 10\%$. This represents an average over 26 individual runs taken on the same day. The data in this case were measured from oscilloscope traces. Corresponding results with the boxcar integrator would be approximately ten times higher because of an additional amplifier in the circuit.

With the mean value of R_0 measured in this set of runs, Eq. (2-25) can be used to calculate $[\text{CO}_2(00^01)]_L^0$. A comparison with the population determined from Eqs. (2-18) and (2-19) can then be made. Such a comparison is shown in Fig. 3.7 for the mean sensitivity quoted above. Agreement is very good for $p_{\text{CO}_2} \leq 0.52 \text{ atm}$. However, additional data at $p_{\text{CO}_2} = 1.02 \text{ atm}$ show a discrepancy of almost 50%. This behavior is to be expected, since at this pressure, Eq. (2-17) is not satisfied.

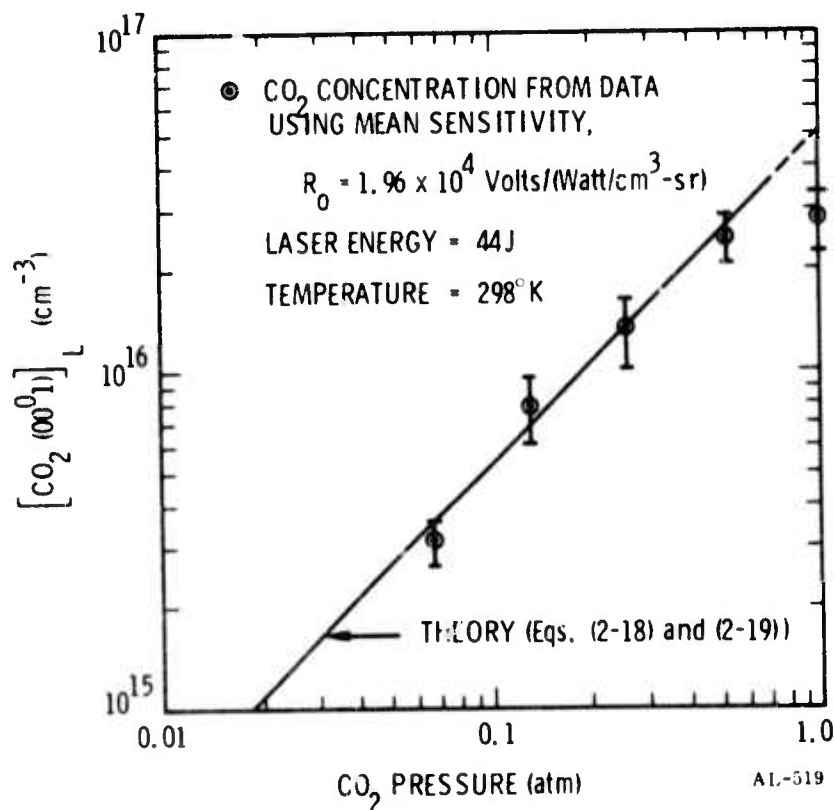


Figure 3.7 - Comparison of Theoretically Predicted $\text{CO}_2(00^01)$ Concentration Due to Saturation With Values Deduced From Data

These results are typical of the CO₂ fluorescence data used to calibrate the detection system. The agreement between theory and experiment on the pressure dependence of the fluorescence intensity, coupled with the measured relaxation time for the decay of that intensity, established the reliability of the calibration technique. Moreover, the consistency of the results, based upon the data taken several weeks apart, was also established. The measured CO₂ ν_3 deactivation rate constant of $k_0 = (1.0 \pm 0.2) \times 10^{-14}$ cm³/sec was averaged over values obtained up to four months apart.

3.3 N₂ Rayleigh Scattering

The N₂ scattering data were obtained with the electronics shown schematically in Fig. 3.4. The boxcar integrator was used at the limit of its duty factor: a 5 μ sec gate width and a laser pulse repetition rate of 1 pps. This required an integration time was 5 min, or 300 laser pulses.

The Rayleigh scattered radiation was superimposed on the wall scattered radiation. Therefore, measurements had to be made with the scattering cell evacuated to 3 torr, and the results then subtracted from those taken with N₂ in the cell. The CO₂ calibration, however, was performed with the boxcar-integrator gate delayed to 10 μ sec. The CO₂ fluorescence in the interval from 10 to 15 μ sec was averaged by the integrator. Since the wall scattered signal decreased to zero by $t = 5$ μ sec, this source of background radiation was not present for the calibration.

If τ_g is the gate width, then the averaged signal for the CO₂ calibration is given by

$$\begin{aligned}\bar{V}_{\text{CO}_2} &= \frac{1}{\tau_g} \int_{t_0}^{t_0 + \tau_g} R_0 \left[\text{CO}_2 (00^0 1) \right]_L S_{\text{CO}_2} e^{-t/\tau} dt \\ &= R_0 \left[\text{CO}_2 (00^0 1) \right]_L S_{\text{CO}_2} \frac{\tau}{\tau_g} e^{-t_0/\tau} \left(1 - e^{-\tau_g/\tau} \right), \quad (3-4)\end{aligned}$$

where, $t_0 = 10 \mu\text{sec}$ is the time at which the gate opens. This expression, with the measured signal strength, determines R_0 . This was done at $p_{\text{CO}_2} = 0.25 \text{ atm}$, where saturation is complete, i.e., $2\sigma \delta E_L / A_L h\nu \sim 3$.

For the N_2 scattering measurements, the laser was operated at 1 pps and 30 to 35 joules per pulse with an unpolarized output. Throughout the series of measurements, laser induced breakdown presented a problem, particularly since the signal integration extended over 300 pulses. Very often, in the middle of a run, breakdown would begin, and once it did, its frequency increased drastically. This necessitated flushing the cell and beginning the run again. Because of this, only two runs were completed successfully at 3 atm and 4 atm of N_2 .

In addition, because of breakdown, the cell had to be completely flushed before changing the pressure in the cell. Simply increasing the pressure from one value to the next produced breakdown on virtually every laser pulse.

For the CO_2 calibration with the boxcar gate delayed by $10 \mu\text{sec}$, the measured signal was typically 10 to 15 mV when the scattering cell was evacuated. With 0.25 atm of CO_2 , the signal \bar{V}_{CO_2} was nominally 100 mV. Thus the boxcar operated on its most sensitive scale, 200 mV full scale. For the N_2 scattering measurements with the boxcar gate delayed by $0.5 \mu\text{sec}$, the measured signal due to wall scattering was typically 600 mV. The ratio of wall scattering to Rayleigh scattering was about 1.0 at 1 atm of N_2 .

The N_2 Rayleigh scattering cross section was determined directly from the measured Rayleigh signal averaged by the boxcar integrator. The cross section is related to the measured signal strength by

$$\begin{aligned} \bar{V}_{\text{Ray}} &= \frac{1}{\tau_g} \int_{t_0}^{t_0 + \tau_g} R_0 [\text{N}_2] \frac{d\sigma}{d\Omega} I_L dt \\ &= \frac{1}{\tau_g} R_0 [\text{N}_2] \frac{d\sigma}{d\Omega} \frac{E_L}{A_L}, \end{aligned} \quad (3-5)$$

where $t_0 = 0.4 \mu\text{sec}$ is the beginning of the laser pulse. The data were taken on different days, and the calibrated responsivity R_0 varied slightly in each case. For ten individual runs, each consisting of 300 laser shots, the mean value of the differential cross section was found to be

$$\frac{d\sigma}{d\Omega} = (2.3 \pm 1.4) \times 10^{-33} \quad \frac{\text{cm}^2}{\text{sr}} \quad (3-6)$$

for cross sections measured at 1 to 4 atm of N_2 . The scatter of the data points about the mean is substantial, amounting to a standard deviation of $\pm 61\%$. The error for each run was estimated to be approximately $\pm 40\%$. This was due primarily to the estimated errors in R_0 (15%), E_L (15%) and A_L (25%).

To our knowledge, the mean value of Eq. (3-6) is the only measured value at $10.6 \mu\text{m}$. However, it can be compared to previously measured cross sections at shorter wavelengths by extrapolating the latter to $10.6 \mu\text{m}$ with the relation $d\sigma/d\Omega \sim \lambda^{-4}$. Such a comparison is given in Table 3.2

TABLE 3.2

COMPARISON OF MEASURED RAYLEIGH SCATTERING CROSS SECTION
AT $10.6 \mu\text{m}$ WITH VALUES EXTRAPOLATED FROM DATA AT 1216A and 6943A

$\frac{d\sigma}{d\Omega} \left(\frac{\text{cm}^2}{\text{sr}} \right)$	Reference	Wavelength at Which Original Data Were Taken
2.3×10^{-33}	Present Work	$10.6 \mu\text{m}$
2.0×10^{-33}	6	6943A
1.0×10^{-33}	17	6943A
6.5×10^{-33}	8	1216A

The cross sections measured by Rudder and Bach,⁽⁶⁾ and by George et al.⁽¹⁷⁾ were with linearly polarized radiation at 6943A, scattered 90° to the laser axis. Therefore, their results had to be converted to the proper value for unpolarized radiation by applying Eqs. (2-8), (2-10) and (2-11). The cross section in Table 3.2 from Gill and Heddle⁽⁸⁾ was calculated from Eq. (2-11) using their measured values of $(n-1)$ and $(6 + 6 \rho_u)/(6 - 7 \rho_u)$ for N_2 at 1216A.

In their published results, Rudder and Bach found excellent agreement between their measured value and the calculated value at 6943A. However, the cross section measured by George et al., was lower than the theoretical value by a factor of two. Consequently, the extrapolated value at $10.6 \mu m$ based upon Rudder and Bach's data appears to be the more reliable of the two.

It would be expected that the cross section due to Gill and Heddle extrapolated to $10.6 \mu m$ would be unreliable, since the extrapolation from 1216A is over eight orders of magnitude. Moreover, N_2 possesses an ultraviolet absorption spectrum which may affect its refractive index, n , at 1216A. Consequently, of the three extrapolated cross sections listed in Table 3.2, the value due to Rudder and Bach appears to provide the most reliable comparison for our measured value. As can be seen, agreement between the two is very good. Rudder and Bach's extrapolated value easily falls within error bounds of the value measured in the present work.

3.4 N_2 Raman Scattering

The measurement program came to an end with no data obtained for N_2 rotational Raman scattering at $10.6 \mu m$. The system sensitivity, measured by the CO_2 calibration and used in the N_2 Rayleigh scattering measurements, was insufficient to permit observation of the Raman scattered component.

As discussed in Section 2, the N_2 Rayleigh cross section is estimated to be approximately 45 times larger than the total Raman band cross section. Therefore, measurement of the Raman scattered radiation with the system described above,

would be impossible with unpolarized incident radiation. As it was, even in the Rayleigh measurements, the boxcar integrator was operated at maximum sensitivity and minimum duty factor. Integration extended over 300 laser pulses.

Unfortunately, the situation with linearly polarized laser radiation was not much improved. As shown in Eq. (2-13), employing polarized laser radiation decreases the Rayleigh component to approximately a factor of 1.6 less than the Raman component. However, the absolute magnitude of the scattered intensity decreases by a factor of 50 (namely, by the depolarization ratio) below the Rayleigh intensity in the unpolarized case. Therefore, for polarized radiation, the Raman signal would be in the 10 mv range, a factor 50 to 60 below wall scattering and a factor of 12 below the generation-recombination noise of the detector.

Moreover, for the laser system used in the experiment, the energy output in the unpolarized mode was approximately twice as great as the pulse energy in the polarized mode. This would have very little practical effect on laser breakdown, so that breakdown in the polarized case would be as troublesome as for the unpolarized Rayleigh measurements described in the previous subsection. However, the decrease in laser energy would decrease the Raman signal to a factor of 24 below the detector noise. To increase this signal-to-noise ratio to unity would require an integration time of approximately 10 min, or 600 laser pulses. Experience with the Rayleigh measurements, however, showed that integrating over more than 200 to 300 laser pulses was virtually impossible with the present system due to the occurrence of breakdown.

Thus, several deficiencies in the experimental apparatus prevented the measurement of the Raman cross section. The responsivity, or sensitivity of the detection system was too low by at least a factor of 50. The laser intracavity power density ($\sim 2 \times 10^8$ watts/cm²) was too close to the breakdown threshold. Finally, the pulse repetition rate of the laser was too low (1 pps) to permit pulse averaging over a reasonable period of time.

4. CONCLUSIONS

This final report discusses the experimental facility constructed to measure the scattering of radiation from room-temperature N_2 at $10.6 \mu m$. The measurements were based upon a calibration of the system by CO_2 fluorescence in the 9.4 and $10.4 \mu m$ bands.

During the calibration, the CO_2 ($00^0 1$) deactivation rate constant was measured to be

$$k_0 = (1.0 \pm 0.2) \times 10^{-14} \quad \frac{cm^3}{sec}$$

at $298^\circ K$. This is in excellent agreement with previously published values by Rosser, Wood and Gerry,^(24,25) and by Moore et al.^(26,27)

Based upon the responsivity determined from the CO_2 calibration, the N_2 Rayleigh scattering cross section for unpolarized radiation at $10.6 \mu m$ was measured as

$$\frac{d\sigma}{d\Omega} = (2.3 \pm 1.4) \times 10^{-33} \quad \frac{cm^2}{sr}$$

This agrees very well with the value measured by Rudder and Bach⁽⁶⁾ at $6943A$ and extrapolated to $10.6 \mu m$ by λ^{-4} . There appear to be no other data available at $10.6 \mu m$ to make a direct comparison with the present result.

The sensitivity of the experimental facility was insufficient to permit measurement of the N_2 Raman cross section. The responsivity was too low by about a factor of 50. Moreover, integration over enough laser pulses to produce an acceptable signal-to-noise ratio was prevented by the presence of laser induced breakdown.

5. ACKNOWLEDGMENTS

The authors wish to acknowledge the skillful assistance of Mr. Conrad M. Gozewski in designing, fabricating and maintaining the major components of the experimental facility.

Preceding page blank

APPENDIX

RADIATIVE LIFETIME IN THE CO₂ 9.4 and 10.4 μm BANDS

The radiative lifetime for a single line in a vibration-rotation band can be expressed in terms of the integrated absorption, α in cm⁻² - atm⁻¹, for the entire band. The lifetime, which is the reciprocal of the Einstein coefficient, is directly related to the integrated intensity for the particular line. Similarly, the integrated line intensity can be written in terms of α .⁽³²⁾ Consequently the radiative lifetime becomes⁽³³⁾

$$\tau_J = \frac{1}{8\pi c} \frac{\omega'}{\omega^3} \left(\frac{N/p}{Q_r} \right) \frac{g_u g_l}{g_L} \frac{1}{|R_{JJ'}^{ll'}|^2} \frac{e^{-E(v_1^l v_2^l v_3^l)/kT}}{(1 - e^{-hc\omega'/kT})} \frac{1}{\alpha(v_1^l v_2^l v_3^l \rightarrow v_1'^l v_2'^l v_3'^l)} \quad (\text{A-1})$$

Here, ω' and ω are the wavenumbers at the band center and line center, respectively; (N/p) is the number density per atm; Q_r is the rotational partition function; g_u and g_L are the statistical weights of the upper and lower levels, respectively; g_l is the l -doubling degeneracy for the lower state; $E(v_1^l v_2^l v_3^l)$ is the energy of the lower state; and v_1 , v_2 , and v_3 are the vibrational quantum numbers of the lower states. The same quantities primed are the corresponding values for the upper state. Finally, $R_{JJ'}^{ll'}$ is the rotational matrix element for the transition, expressed in terms of the rotational quantum number, J .

For a given temperature, the lifetime for a particular line can be determined from Eq. (A-1) if the integrated band intensity α is known at the same temperature. Fortunately, for the 9.4 and 10.4 μm bands of CO₂, such data exist. Moreover, measured values of the lifetimes of the P(20) line in each band have recently been published.⁽²²⁾ For each P(20) line, $\tau_r = 5.0$ sec. From Eq. (A-1) this corresponds to

Preceding page blank

$$(10^0 0 - 00^0 1) = 1.92 \times 10^{-2} \text{ cm}^{-2} \text{ atm}^{-1}$$

$$(02^0 0 - 00^0 1) = 2.55 \times 10^{-2} \text{ cm}^{-2} \text{ atm}^{-1}$$

which is in good agreement with published values.⁽³⁴⁻³⁷⁾

The radiative lifetimes for the two bands as calculated from Eq. (A-1) are shown in Fig. A.1. Results for the P and R branches of each band are given as a function of rotational quantum number of the lower state. The calculated values for the 9.4 μm band are almost identical to those of the 10.4 μm band.

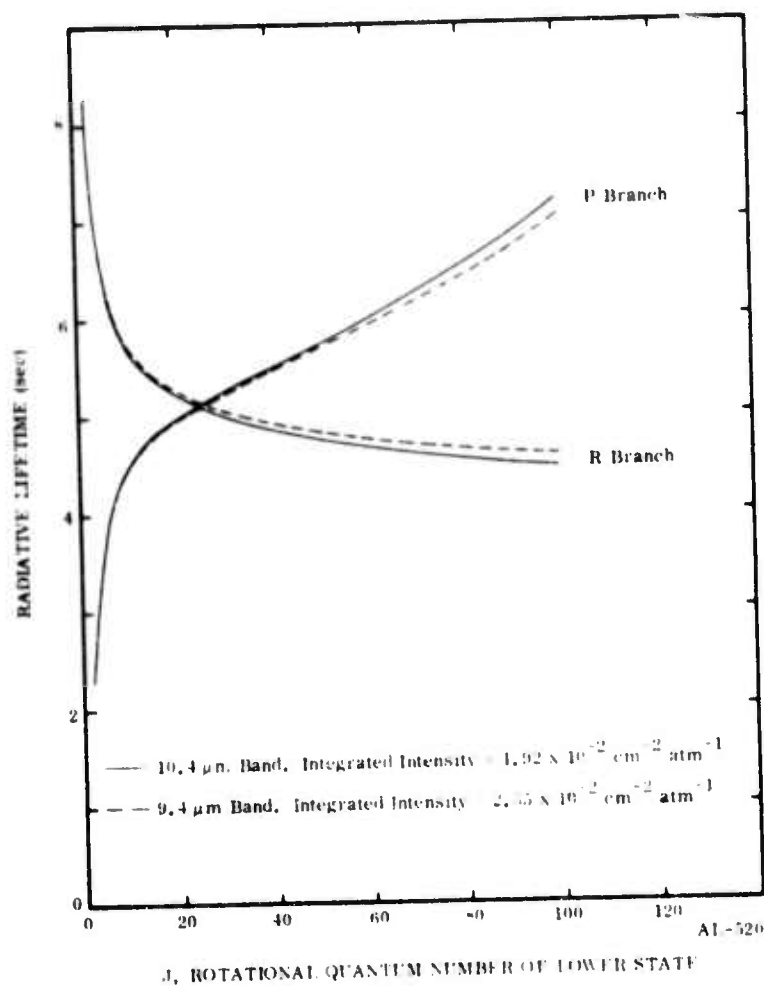


Figure A.1 - Radiative Lifetime of the 9.4 and 10.4 μm Bands of CO_2

Using the results of Fig. A.1 with the proper wavelength for each line and with the equilibrium population distribution for the CO_2 (00^0_1) rotational levels, the CO_2 emission function, S_{CO_2} , defined in Eq. (2-24) was calculated. At 298°K ,

$$S_{\text{CO}_2} = 1.24 \times 10^{-21} \quad \frac{\text{watts}}{\text{sr}} .$$

However, if we assume the radiative lifetime for each rotational is $\tau_r = 5$ sec, and if we use a mean wavelength, $\bar{\lambda} = 10 \mu\text{m}$, for each line, then S_{CO_2} is given by

$$S_{\text{CO}_2} = \frac{4hc}{4\pi\lambda\tau_r} = 1.27 \times 10^{-21} \quad \frac{\text{watts}}{\text{sr}} .$$

This differs from the results in Eq. (2-24) by 2% . Because of its simplicity, this expression was used in the CO_2 calibration analysis.

REFERENCES

1. H.A. Hyatt, J.M. Cherlow, W.R. Fenner, and S.P.S. Porto, "Cross Section for the Raman Effect in Molecular Nitrogen Gas," J. Opt. Soc. Am. **63**, 1604 (1973).
2. C.M. Penney, R.A. St. Peters, and M. Lapp, "Absolute Rotational Raman Cross Sections for N₂, O₂, and CO₂," J. Opt. Soc. Am. **64**, 712 (1974).
3. G. Placzek, Handbuch der Radiologie, Vol. 6, G. Marx (Ed.), (Akademische Verlagsgesellschaft, Leipzig (1934), Part 2, p. 205 (Translated by A. Werbit as UCRL Translation No. 526(1), Lawrence Radiation Laboratory (1959)).
4. S.D. Silverstein, "Absolute Rotational Raman Cross Sections for Scheneectady, N.Y., N₂ and O₂ from the Far Infrared to the Ultraviolet," General Electric Co., Corporate Research and Development Report No. 73 CRD007 (1962).
5. G. Herzberg, Molecular Spectra and Molecular Structure, Vol. 1, Spectra of Diatomic Molecules, 2nd ed., Van Nostrand, New York (1950), p. 128.
6. R.R. Rudder and D.R. Bach, "Rayleigh Scattering of Ruby Laser Light by Neutral Gases," J. Opt. Soc. Am. **58**, 1260 (1968).
7. C.M. Penney, "Light Scattering in Terms of Oscillator Strengths and Refractive Indices," J. Opt. Soc. Am. **59**, 34 (1969).
8. P. Gill and D.W.O. Heddle, "Determination of the Refractive Indices of Gases in the Vacuum Ultraviolet. II. The Rayleigh Scattering Method," J. Opt. Soc. Am. **53**, 847 (1963).
9. S. Chandasekhar, Radiative Transfer, Dover, New York (1960), p. 38.
10. A. Weber, S.P.S. Porto, L.E. Cheesman, and J.J. Barrett, "High Resolution Raman Spectroscopy of Gases with CW-Laser Excitation," J. Opt. Soc. Am. **57**, 19 (1967).
11. N. J. Bridge and A.D. Buckingham, "Polarization of Laser Light Scattered by Gases," J. Chem. Phys. **40**, 2733 (1964).
12. W.R. Fenner, H.A. Hyatt, J.M. Kellam, and S.P.S. Porto, "Raman Cross Section of Some Simple Gases," J. Opt. Soc. Am. **63**, 73 (1973).

Preceding page blank

References (Cont.)

13. C.M. Penney, L.M. Goldman, and M. Lapp, "Raman Scattering Cross Sections," Nature Phys. Sci. **235**, 110 (1972).
14. D.G. Fouche and R.K. Chang, "Relative Raman Cross Section for O_3 , CH_4 , C_3H_8 , NO , N_2O and H_2 ," Appl. Phys. Lett. **20**, 256 (1972).
15. W.F. Murphy, W. Holzer, and H.J. Bernstein, "Gas Phase Raman Intensities: A Review of 'Pre-Laser' Data," Appl. Spectrosc. **23**, 211 (1969).
16. E.J. Stansbury, M.F. Crawford, and H.L. Welch, "Determination of Rates of Change of Polarizability from Raman and Rayleigh Intensities," Can. J. Phys. **31**, 951 (1953).
17. T.V. George, L. Goldstein, L. Slasma, and M. Yokoyama, "Molecular Scattering of Ruby-Laser Light," Phys. Rev. **137**, A369 (1965).
18. K.S. Jammu, G.E. St. John, and H.L. Welsh, "Pressure Broadening of the Rotational Raman Lines of Some Simple Gases," Can. J. Phys. **44**, 797 (1966).
19. S.A. Munjee and W.H. Christiansen, "Mixed Mode Contributions to Absorption in CO_2 at 10.6μ ," Appl. Opt. **12**, 993 (1973).
20. R.L. Taylor and S. Bitterman, "Survey of Vibrational Relaxation Data for Processes Important in the CO_2 - N_2 Laser System," Rev. Mod. Phys. **41**, 26 (1969).
21. J.A. Blauer and G.R. Nickerson, "A Survey of Vibrational Relaxation Rate Data for Processes Important to CO_2 - N_2 - H_2O Infrared Plume Radiation," Air Force Rocket Propulsion Laboratory, Edwards AFB, Calif., Technical Report No. AFRPL-TR-73-57 (October 1973).
22. E.R. Murray, C. Kruger, and M. Mitchner, "Measurement of 9.6μ CO_2 Laser Transition Probability and Optical Broadening Cross Section," Appl. Phys. Lett. **24**, 180 (1974).
23. D.F. Eggers and B.L. Crawford, J., "Vibrational Intensities. III. Carbon Dioxide and Nitrous Oxide," J. Chem. Phys. **19**, 1554 (1951).
24. W.A. Rosser, J., A.D. Wood, and E.T. Gerry, "Deactivation of Vibrationally Excited Carbon Dioxide (ν_2) by Collisions with Carbon Dioxide or with Nitrogen," J. Chem. Phys. **50**, 4996 (1969).
25. W.A. Roser, J., and E.T. Gerry, "De-excitation of Vibrationally Excited CO_2 (00^0_1) by Collisions with CO_2 , H_2 , NO and Cl_2 ," J. Chem. Phys. **54**, 4131 (1971).

References (Cont.)

26. C.B. Moore, R.E. Wood, B-L. Hu, and J.T. Yardley, "Vibrational Energy Transfer in CO₂ Lasers," J. Chem. Phys. **46**, 4222 (1967).
27. J.C. Stephenson and C.B. More, "Near-Resonant Vibration \rightarrow Vibration Energy Transfer: CO₂ ($\nu_3 = 1$) + M \rightarrow CO₂ ($\nu_1 = 1$) + M* + ΔE ," J. Chem. Phys. **52**, 2333 (1970).
28. M. Camac and R.C. Sepucha, "The Measurement of the Rotational Raman Cross Section of Atmospheric Constituents at 10.6 Microns," Aerodyne Research, Inc., Burlington, Massachusetts, Report No. ARI-RR-32.1 (August 1973).
29. R.E. Schlier, A.N. Pirri, and D.J. Reilly, "Air Breakdown Studies," Air Force Weapons Laboratory, Air Force Systems Command, Kirtland AFB, N.M., Technical Report No. AFWL-TR-72-74 (February 1973).
30. S.S. Penner, R.C. Sepucha, and J.E. Lowder, "Approximate Calculations in Infrared Vibration-Rotation Spectra," J. Quant. Spectrosc. Radiat. Transfer **10**, 1001 (1970).
31. C. Young and R.E. Chapman, "Line Widths and Band Strengths for the 9.4 - and 10.4- μ m CO₂ Bands," J. Quant. Spectrosc. Radiat. Transfer **14**, 679 (1974).
32. S.S. Penner, Quantitative Molecular Spectroscopy and Gas Emissivities, Chapt. 7. Addison Wesley, Reading, Massachusetts 1959.
33. R.C. Sepucha, "CO₂ Radiative Lifetimes in the 15-Micron Region," Aerodyne Research, Inc. Burlington, Massachusetts, Report No. ARI-LR-28.1 (December 1973).
34. B. Schurin and R.E. Ellis, "Total Intensity Measurements for the CO₂ Band in the 961 - cm⁻¹ and 1061 - cm⁻¹ Regions," Appl Opt. **9**, 223 (1970).
35. T.K. McCubbin, Jr. and T.R. Mooney, "A Study of the Strengths and Widths of Lines in the 9.4 and 10.4 μ CO₂ Bands," J. Quant. Spectrosc. Radiat. Transfer **8**, 1255 (1968).
36. L.D. Gray, "Calculations of Carbon Dioxide Transmission Part I - The 9.4 μ and 10.4 μ Bands," J. Quant. Spectrosc. Radiat. Transfer **7**, 143 (1967).
37. S.R. Drayson and C. Young, "Band Strength and Line Half-Width of the 10.4 μ CO₂ Band," J. Quant. Spectrosc. Radiat. Transfer **7**, 993 (1967).